S/N and Error Rate Performance in AlGaAs Semiconductor Laser Preamplifier and Linear Repeater Systems

TAKAAKI MUKAI, YOSHIHISA YAMAMOTO, MEMBER, IEEE, AND TATSUYA KIMURA, SENIOR MEMBER, IEEE

Abstract—**The applications of AlGaAs semiconductor laser preamplifier and linear repeaters in single mode optical fiber transmission systems were studied through the baseband signal-to-noise ratio and bit error rate performance measurement. Experiments were carried out with the Fabry-Perot cavity laser amplifiers whose characteristics are improved by reducing the input mirror reflectivity to 6 percent. The use of a preamplifier improves the minimum detectable power by 7.4 dB over the Si-APD direct detection level when the received signal is amplified by 30 dB before photodetection. The use of two linear repeaters increases the regenerative repeater gain by 37 dB. These experimental results are in good agreement with theoretical predictions based on the photon statistic master equation analysis.**

I. INTRODUCTION

SEMICONDUCTOR laser amplifiers have been studied extensively in the last few years due to their potential possibilities for optical fiber transmission system application. Semiconductor laser preamplifiers can improve the minimum detectable power over a conventional avalanche photodiode (APD) direct detection scheme [1]. When they are used as optical repeaters in IM direct detection systems [1], [2] and in coherent systems [3], [4], they can serve to expand the regenerative repeater spacing. They can also be used as booster amplifiers to compensate for the insertion loss and power splitting loss in optical circuits.

Preamplifier performance for a Fabry-Perot (FP) cavity AlGaAs laser amplifier was reported for a 100 Mbit/s PCM-IM signal with a less than 10 dB signal gain [5]. Noise characteristics [1], [6]-[8] for AlGaAs laser amplifiers, as well as their signal gain [9], [10], frequency bandwidth [10], and saturation output power [10], have been elucidated theoretically and experimentally. These characteristics can be improved by reducing the facet reflectivities and cavity length [10]. As for the noise characteristics, an asymmetrical cavity configuration with low-input and high-output mirror reflectivities is superior to that with high-input and low-output mirror reflectivities [8].

This paper describes baseband signal-to-noise ratio (S/N) and bit error rate characteristics for AlGaAs laser preamplifier and linear repeater systems. Baseband S/N in the optical direct amplification systems is formulated based on the photon statistic master equation analysis extended to FP cavity laser amplifiers [1]. They are compared to experimental results obtained by using AlGaAs laser amplifiers. Noise parameters are expressed analytically in terms of amplifier structural and material parameters. Amplifier characteristics such as signal gain, frequency bandwidth, and saturation output power were measured for the noise-improved AlGaAs laser amplifier which has input and output mirror reflectivities of 6 and 32 percent, respectively. Noise parameters are also calculated as a function of the signal gain.

The optical preamplifier system performance was studied for a 100 Mbit/s PCM-IM signal with various signal gains up to 30 dB. The baseband S/N and error rate dependences on the received power were measured for the AlGaAs laser preamplifier followed by an Si-APD. Results were compared to that for the Si-APD direct detection scheme.

A linear optical repeater system is demonstrated for a 100 Mbit/s PCM-IM signal using two AlGaAs laser amplifiers in tandem. The baseband S/N and error rate dependences on the received power were measured at various signal levels, both in front of and behind the first and the second repeaters.

II. BASEBAND SIGNAL-TO-NOISE RATIO FORMULATION

A. Preamplifier System

The mean and variance values in the photon number per second at the FP cavity preamplifier output $\langle n_{out}\rangle$ and σ^2_{out} $(=\langle n^2_{out}\rangle - \langle n_{out}\rangle^2)$ are [1]

$$\langle n_{out}\rangle = G\langle n_{in}\rangle + (G-1)\, n_{sp} m_t \Delta f_1 \tag{1}$$

$$\sigma^2_{out} = G\langle n_{in}\rangle + (G-1)\, n_{sp} m_t \Delta f_1 + 2G(G-1)\, n_{sp}\chi\langle n_{in}\rangle + (G-1)^2 n^2_{sp} m_t \Delta f_2 + G^2(\langle n^2_{in}\rangle - \langle n_{in}\rangle^2 - \langle n_{in}\rangle). \tag{2}$$

Here, $\langle n_{in}\rangle$ is the mean value of the photon number per second incident on the preamplifier, G is the signal gain at resonant condition, Δf_1 and Δf_2 are, respectively, the equivalent noise bandwidths for the spontaneous emission shot noise and the beat noise between spontaneous emission components, χ is the excess noise coefficient for the beat noise between signal and spontaneous emission, m_t is the effective number of transverse modes, and n_{sp} is the population inversion parameter of the amplifying medium. Two terms on the right-hand side of (1) represent amplified signal and spontaneous emission, respectively. Five terms on the right-hand side of (2) represent amplified signal shot noise, spontaneous emission

Manuscript received March 8, 1982; revised June 3, 1982.

The authors are with Musashino Electrical Communication Laboratory, Nippon Telegraph and Telephone Public Corporation, Musashino-shi, Tokyo 180, Japan.

0018-9480/82/1000-1548$00.75

shot noise, beat noise between signal and spontaneous emission, beat noise between spontaneous emission components, and signal excess noise, respectively. The last term disappears when the input signal is completely coherent.

Equivalent noise bandwidth Δf_1 for the spontaneous emission shot noise is given by [1]

$$\Delta f_1 = \sum_{m_l} \frac{(1+R_1G_s)(1-R_2)(G_s-1)}{1-R_1R_2G_s^2} \cdot \left(\frac{C_0}{2\mathcal{L}}\right) \Big/ (G-1) \quad (3)$$

where signal gain G for the central longitudinal mode at resonant condition is

$$G = \frac{(1-R_1)(1-R_2)G_s^0}{(1-\sqrt{R_1R_2}G_s^0)^2}. \quad (4)$$

Here, R_1 and R_2 are, respectively, input and output mirror reflectivities, G_s^0 is the single-pass gain for the central longitudinal mode, G_s is the single-pass gain for the other longitudinal modes, C_0 is the light velocity in the amplifying medium, and $\mathcal{L}$ is the amplifier length. Spontaneous emission shot noise is obtained by the summation of the number of spontaneous photons in a single longitudinal mode over the total of the longitudinal modes m_l. The spectrum width for a positive net gain is determined by Stern's gain calculation results [11].

Equivalent noise bandwidth Δf_2 for the beat noise between spontaneous emission components is given by [1]

$$\Delta f_2 = \sum_{m_l} \frac{(1+R_1G_s)^2(1-R_2)^2(G_s-1)^2(1+R_1R_2G_s^2)}{(1-R_1R_2G_s^2)^3} \cdot \left(\frac{C_0}{2\mathcal{L}}\right) \Big/ (G-1)^2. \quad (5)$$

Spontaneous-spontaneous beat noise is obtained by the summation of the overlap integral of the number of spontaneous photons in a single longitudinal mode.

Excess noise coefficient χ for the beat noise between signal and spontaneous emission is given by [1]

$$\chi = \frac{(1+R_1G_s^0)(1-R_2)(G_s^0-1)}{(1-\sqrt{R_1R_2}G_s^0)^2} \Big/ (G-1) \quad (6)$$

and in the case of $G \gg 1$

$$\chi \cong \frac{(1+R_1G_s^0)(G_s^0-1)}{(1-R_1)\cdot G_s^0}. \quad (7)$$

Signal-spontaneous beat noise is obtained by the product of the number of signal photons and the number of spontaneous photons at the cavity resonant frequency. χ represents the signal-spontaneous beat noise enhancement due to the input mirror reflectivity in the FP cavity amplifier.

Maximum gain coefficient $g(\mathrm{cm}^{-1})$ is approximated as a linear function of the minority carrier density N_e as follows [11]:

$$g = (A/C_0)(N_e - N_0) \quad (8)$$

where N_0 is the minority carrier density at which the stimulated emission becomes equal to the stimulated absorption. Material parameters A and N_0 are 2.82×10^{-6} (cm^3/s) and 1.36×10^{18} (cm^{-3}), respectively, nondoped AlGaAs lasers [12]. Single-pass gain G_s^0 is related to the gain coefficient g by

$$G_s^0 = \exp[(\Gamma g - \alpha)\mathcal{L}] \quad (9)$$

where Γ is the mode confinement factor and α is the loss coefficient. From (8) and (9), population inversion parameter n_{sp} is given by

$$n_{sp} \equiv \frac{N_e}{N_e - N_0} = 1 + \frac{A\Gamma N_0}{C_0\{\alpha + (1/\mathcal{L})\cdot \ln G_s^0\}}. \quad (10)$$

n_{sp} represents the degradation of available carrier density from the injected value due to the existence of the stimulated absorption. For the ideal amplifier with traveling-wave (TW) type ($R_1 = R_2 = 0$), in which no stimulated absorption occurs, n_{sp} and χ are equal to 1, and both Δf_1 and Δf_2 are determined by the optical gain bandwidth.

Consider an optical receiver system in which an intensity-modulated optical signal is incident on an FP cavity laser amplifier, followed by APD and a baseband electronic amplifier. The preamplifier output is detected by the APD with quantum efficiency η_D, avalanche multiplication factor $\langle g\rangle$, and excess noise exponent x. The coupling efficiency between the amplifier and APD is η_c. From (1), baseband signal power is expressed by $(2G\langle n_{\mathrm{in}}\rangle e\eta_c\eta_D\langle g\rangle)^2 R_L$. The baseband noise power generated in a unit load resistance per unit bandwidth is expressed by $e^2\sigma_{\mathrm{out}}^2$, which corresponds to the noise power measured by the PD detection ($\langle g\rangle = 1$) with unity coupling and quantum efficiencies ($\eta_c\eta_D = 1$). The variance of photon number σ_{out}^2 is given by (2). When the APD is used under the multiplication condition ($\langle g\rangle \geq 1$) with less than unity coupling and quantum efficiencies ($\eta_c\eta_D < 1$), baseband shot noise and beat noise are proportional to $\eta_c\eta_D\langle g\rangle^{2+x}$ and $(\eta_c\eta_D\langle g\rangle)^2$, respectively [8]. Besides the above photon noise, electronic amplifier thermal noise $4k_B\mathrm{T}F_tB_0$ is also added. Baseband *S/N* is expressed as follows:

$$S/N = (2\langle n_{\mathrm{in}}\rangle)^2 \Big/ \left\{2\left(\langle n_{\mathrm{in}}\rangle + \frac{G-1}{G}\cdot n_{sp}m_t\Delta f_1\right)\frac{\langle g\rangle^x}{\eta_c\eta_D G} + 2\frac{G-1}{G}\cdot n_{sp}\chi\langle n_{\mathrm{in}}\rangle + \left(\frac{G-1}{G}\right)^2 n_{sp}^2 m_t\Delta f_2 + \frac{4k_B\mathrm{T}F_t}{R_L(e\eta_c\eta_D\langle g\rangle G)^2}\right\}\cdot B_0. \quad (11)$$

Here, B_0 is baseband filter bandwidth, F_t is baseband amplifier noise figure, R_L is photodetector load resistance, e is electron charge, and k_B is Boltzmann's constant. Under the condition that preamplifier signal gain G is large enough and APD gain $\langle g\rangle$ is optimized, shot noise and thermal noise can be neglected, compared to the beat noise generated in the optical preamplifier. Baseband *S/N* is approximated as follows:

$$S/N \cong \frac{(2\langle n_{\mathrm{in}}\rangle)^2}{(2n_{sp}\chi\langle n_{\mathrm{in}}\rangle + n_{sp}^2 m_t\Delta f_2)\cdot B_0}. \quad (12)$$

Coupling efficiency η_c between the preamplifier and detector surface must be maximized to prevent impairing the beat noise limited detection in the optical preamplifier scheme.

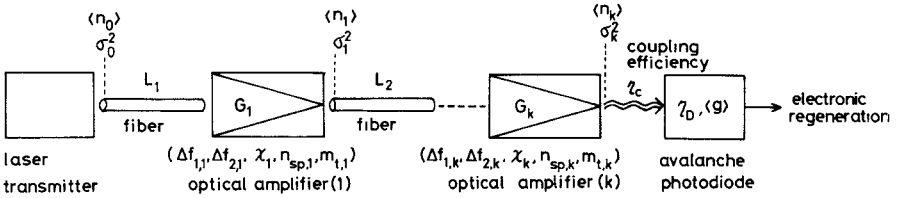

Fig. 1. Optical repeater system using FP optical linear amplifiers whose gains and noise parameters differ from each other. Here, L is the fiber loss and $\langle n_k \rangle$ is the number of kth repeater output photons.

B. Linear Repeater System

Consider an optical linear repeater system shown in Fig. 1, in which the attenuated intensity-modulated signal due to fiber loss L_i is recovered by gain G_i for the ith FP cavity amplifier. The mean and variance values in the number of output photons from the kth amplifier are calculated by using (1) and (2) iteratively.

$$\langle n_k \rangle = \langle n_0 \rangle \cdot \prod_{i=1}^{k} (L_i G_i) + \sum_{i=1}^{k} \left\{ (G_i - 1)\, n_{sp,i} m_{t,i} \Delta f_{1,i} \cdot \prod_{j=i+1}^{k} (L_j G_j) \right\} \tag{13}$$

$$\begin{aligned} \sigma_k^2 = {} & \langle n_0 \rangle \cdot \prod_{i=1}^{k} (L_i G_i) + \sum_{i=1}^{k} \left\{ (G_i - 1)\, n_{sp,i} m_{t,i} \Delta f_{1,i} \cdot \prod_{j=i+1}^{k} (L_j G_j) \right\} + \sum_{i=1}^{k} \left[2 \left\{ \langle n_0 \rangle \cdot \prod_{j=1}^{i} (L_j G_j) \right\} \cdot (G_i - 1)\, n_{sp,i} \chi_i \cdot \prod_{j=i+1}^{k} (L_j G_j)^2 \right] \\ & + \sum_{i=1}^{k} \left\{ (G_i - 1)^2 n_{sp,i}^2 m_{t,i} \Delta f_{2,i} \cdot \prod_{j=i+1}^{k} (L_j G_j)^2 \right\} + 2 \sum_{i=1}^{k-1} (G_i - 1) n_{sp,i} m_{t,i} \Delta f_{1,i} \cdot \left[\sum_{j>i}^{k} \left\{ \prod_{l=i+1}^{j} (L_l G_l) \right\} (G_j - 1)\, n_{sp,j} \chi_j \cdot \left\{ \prod_{m=j+1}^{k} (L_m G_m)^2 \right\} \right] + (\sigma_0^2 - \langle n_0 \rangle) \cdot \prod_{i=1}^{k} (L_i G_i)^2 \end{aligned} \tag{14}$$

where $\langle n_0 \rangle$ and σ_0^2 are the mean and variance values in the number of the output photons from the laser transmitter. The fourth and fifth terms on the right-hand side of (14) are both the beat noise between spontaneous emission components. The former is induced between spontaneous emission components within the ith amplifier itself. The latter is induced between spontaneous emission of the ith amplifier and that of all the following amplifiers.

Assuming that all amplifiers have the same signal gain G and noise parameters Δf_1, Δf_2, χ, n_{sp}, m_t, and that fiber loss L is set to be constant G^{-1} between any two repeaters, we have

$$\langle n_k \rangle = \langle n_0 \rangle + (G - 1)\, n_{sp} \Delta f_1 (k + m_t - 1) \tag{15}$$

$$\begin{aligned} \sigma_k^2 = {} & \langle n_0 \rangle + (G - 1)\, n_{sp} \Delta f_1 (k + m_t - 1) + 2(G - 1)\, n_{sp} \chi k \langle n_0 \rangle + (G - 1)^2 n_{sp}^2 \cdot \{ \Delta f_2 (k + m_t - 1) + \Delta f_1 \chi k (k - 1) \} + (\sigma_0^2 - \langle n_0 \rangle). \end{aligned} \tag{16}$$

Here, each effective transverse mode number for the spontaneous emission noise of up to the $(k-1)$th repeater is determined to be 1 because single mode fiber couples only one transverse mode.

When an optically repeatered intensity-modulated signal at the kth repeater output is detected by an APD with coupling efficiency η_c, baseband S/N is expressed in terms of the input photon number per second $\langle n_{in} \rangle$ $(= \langle n_0 \rangle / G)$ to the repeater amplifier as follows:

$$\begin{aligned} S/N = {} & (2\langle n_{in} \rangle)^2 \Big/ \left[2 \left\{ \langle n_{in} \rangle + \frac{G - 1}{G} \cdot n_{sp} \Delta f_1 (k + m_t - 1) \right\} \cdot \frac{\langle g \rangle^x}{\eta_c \eta_D G} + 2 \frac{G - 1}{G} \cdot n_{sp} \chi k \langle n_{in} \rangle + \left(\frac{G - 1}{G} \right)^2 n_{sp}^2 \{ \Delta f_2 (k + m_t - 1) + \Delta f_1 \chi k (k - 1) \} + \frac{4 k_B \mathrm{TF}_t}{R_L (e \eta_c \eta_D \langle g \rangle G)^2} \right] \cdot B_0. \end{aligned} \tag{17}$$

Under the condition that repeater gain G is large enough and APD gain $\langle g \rangle$ is optimized, and that coupling efficiency η_c is large enough, shot noise and baseband amplifier thermal noise can be neglected, compared to two beat noises generated in the optical repeaters. Baseband S/N can be approximated by

$$S/N \cong \frac{(2\langle n_{in} \rangle)^2}{[2 n_{sp} \chi k \langle n_{in} \rangle + n_{sp}^2 \cdot \{ \Delta f_2 (k + m_t - 1) + \Delta f_1 \chi k (k - 1) \}] \cdot B_0}. \tag{18}$$

Two beat noise components decrease with η_c^2, while shot noise decreases with η_c [8]. When η_c becomes small, baseband S/N is determined by the shot noise and the thermal noise.

In a preamplifier system in which a weak signal is received, baseband S/N is dominated by the spontaneous-spontaneous beat noise determined by $n_{sp}^2 \Delta f_2$. On the contrary, baseband S/N in the repeater system, where the signal level is set near

the saturation output power, is dominated by the signal-spontaneous beat noise determined by $n_{sp}\chi k$.

In the ideal repeater system, baseband *S/N* just after the kth ideal amplifier with TW operating in theoretical signal-spontaneous beat noise limit is expressed in simple form as

$$(S/N)_{\text{ideal}} = 2\langle n_{\text{in}}\rangle/k \cdot B_0. \tag{19}$$

In the case of $k = 1$, (19) is identical to the ideal *S/N* with theoretical shot noise limit in the direct detection scheme.

S/N degradation D from that realized by the ideal laser amplifier with theoretical shot noise limit is expressed as follows:

$$D \equiv \frac{(S/N)_{\text{ideal}}}{S/N} \cong n_{sp}\chi + \frac{n_{sp}^2\{\Delta f_2 + \Delta f_1\chi(k-1)\}}{2\langle n_{\text{in}}\rangle}. \tag{20}$$

S/N degradation in the linear repeater system with low signal level operation increases with increasing the number of repeaters k due to the accumulation of the spontaneous-spontaneous beat noise. D can be decreased to $n_{sp}\chi$ by increasing the input signal level.

III. Signal Gain, Frequency Bandwidth, Saturation Output Power, and Noise Characteristics

The laser amplifier has the same structure as a CSP laser [13] emitting at 825 nm. It has a 300 μm cavity length. The input facet is antireflection coated and the resultant reflectivity is 6 percent. The output facet is not coated and it has 32 percent reflectivity. Amplifier experiments were carried out with a dc bias current just below its oscillation threshold.

Signal gain dependences on injection current, input optical frequency, and optical signal power level were measured. Signal gain measurement was carried out by the optical signal injection method, using the same experimental setup shown in Fig. 1 in [10].

Unsaturated signal gain for the TE-polarized signal at resonant condition is shown in Fig. 2 as a function of the pumping rate J/J_{th}. The resonant signal gain increases with the pumping rate up to 33 dB at $J/J_{th} = 1$. Maximum available signal gain is increased by about 7 dB by reducing the input mirror reflectivity [10].

The half bandwidth between 3 dB points (HWHP) $\Delta\nu_{1/2}$ for signal gain versus signal gain G at the center frequency is shown in Fig. 3. Experimental results are in good agreement with the theoretical curve given by (19) in [10]. The root-gain bandwidth product $\sqrt{G}B$ for this amplifier is 43 GHz, which is 1.8 times as large as that of the noncoated amplifier [10].

Signal gain at resonant condition versus amplified output power P_{out} is shown in Fig. 4. Unsaturated signal gains of 20.2, 25, and 30.4 dB obtained at 0.94, 0.966, and 0.99 pumping rate, respectively, decrease with the amplified output power. Saturation output power $P_{3\text{ dB}}$, at which the signal gain is decreased by 3 dB from the unsaturated value, decreases with increasing the unsaturated signal gain [9]. Saturation output powers corresponding to the above signal gains are -4.4, -6.4, and -8.6 dBm, respectively. Saturation

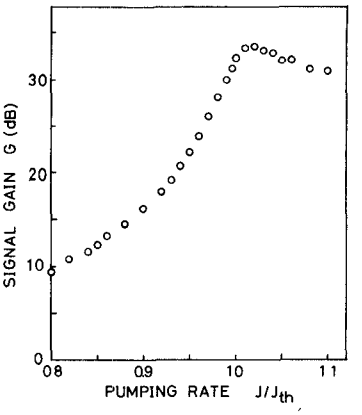

Fig. 2. Unsaturated signal gain G versus amplifier pumping rate J/J_{th}.

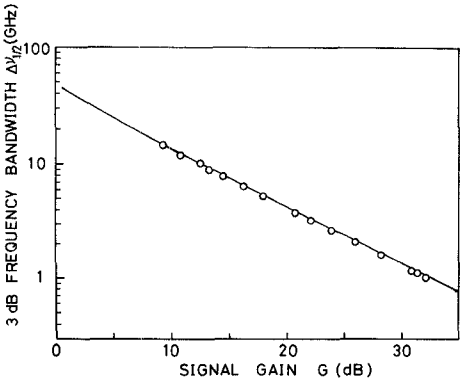

Fig. 3. 3 dB down frequency half bandwidth versus signal gain at resonant frequency.

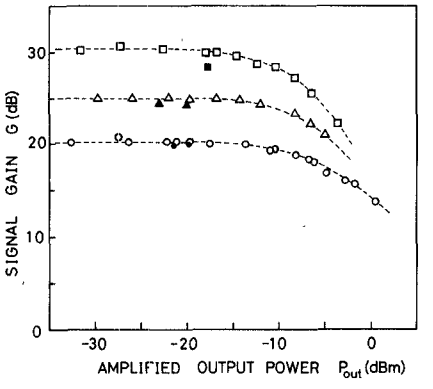

Fig. 4. Signal gain G versus amplified output power P_{out}. Open and filled marks were measured for dc input signal and for IM-FM input signal, respectively.

output power for a 20 dB signal gain is increased by 2.6 dB by reducing the input mirror reflectivity.

Equivalent noise bandwidths Δf_1 and Δf_2 versus the signal gain bandwidth product $\sqrt{G}B$ for this amplifier is 43 GHz, (5), respectively. Δf_1 is wider than Δf_2 by a factor of 3. They decrease with increasing signal gain in the range between 10^{10} and 10^{13}. They can be reduced by 10-16 dB to the full gain bandwidth (FWHP) using the narrow-band optical filter to select the gain central longitudinal mode.

Excess noise coefficient χ, population inversion parameter n_{sp}, and effective transverse mode number m_t are shown in Fig. 6 as a function of the signal gain. χ and n_{sp} are calculated

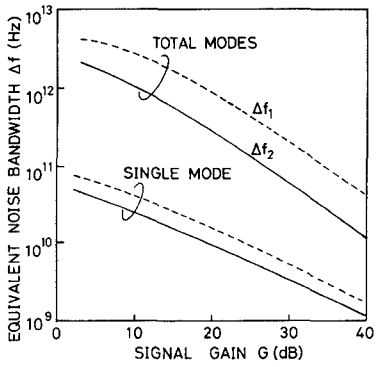

Fig. 5. Equivalent noise bandwidth Δf_1 and Δf_2 versus signal gain G.

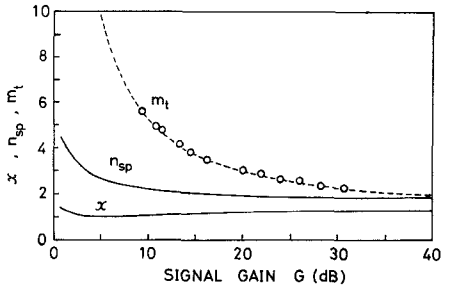

Fig. 6. Excess noise coefficient χ, population inversion parameter n_{sp}, and effective transverse mode number m_t versus signal gain G.

using (6) and (10), respectively. Loss coefficient α is assumed to be 10 cm^{-1} [13]. χ and n_{sp} have constant values of 1.2 and 1.9, respectively, above 10 dB signal gain. m_t is derived from the measured photodetector initial photocurrent $\langle i_{ph0} \rangle$ corresponding to the spontaneous emission shot noise given by

$$\langle i_{ph0} \rangle = e(G - 1)\, n_{sp} m_t \Delta f_1 \eta_c \eta_D. \tag{21}$$

m_t decreases with signal gain and approaches 2, which corresponds to single transverse mode operation with TE and TM polarization.

IV. Preamplifier Performance

An intensity-modulated laser and the amplifier are decoupled by an optical isolator. They are temperature controlled within ±0.02°C. The signal source oscillator is biased at $J/J_{th} = 1.3$, and is modulated by a sinusoidal current at 100 MHz in the S/N measurement or by a nonreturn-to-zero (NRZ) pulse current at 100 Mbits/s in the error rate measurement. Modulation depth m is kept at 0.62–0.75 in order to maintain the single longitudinal mode operation. The amplified optical signal is detected under the optimized avalanche gain condition, using an Si-APD with excess noise exponent $x = 0.5$ and quantum efficiency $\eta_D = 0.7$.

The signal and noise powers are measured by a spectrum analyzer after the baseband amplifier with 16–36 dB gain and 4 dB noise figure. Measured rms signal power is converted to the pulse peak signal power. Assuming that the noise bandwidth is 75 MHz for the 100 Mbit/s data rate, baseband S/N is obtained using both the pulse peak signal power and measured noise power. Baseband S/N for a 100 Mbit/s PCM-IM signal versus amplified average signal is shown in Fig. 7 for the 20, 25, and 30 dB signal gain. In the low-input signal region, where the dominant noise is signal-independent beat noise between spontaneous emission components [8], baseband S/N increases with the amplified signal level by P_{out}^2. In the high-input signal region, where the dominant noise is signal-dependent beat noise between signal and spontaneous emission [8], baseband S/N is proportional to amplified signal level P_{out}. For high amplified signal level $P_{out} > -10$ dBm, baseband S/N has a constant value due to the signal gain saturation.

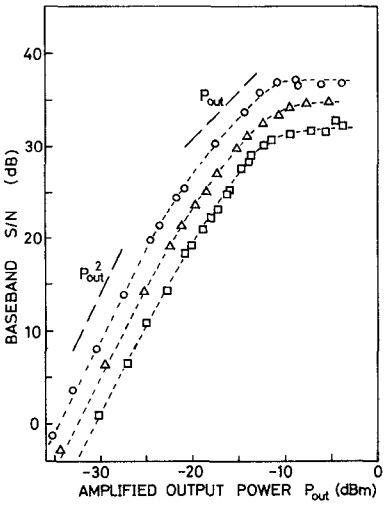

Fig. 7. Baseband S/N versus amplified average signal level P_{out}. Experimental results ($m = 0.68$, $\eta_c = -4$ dB). ○: 20 dB; △: 25 dB; □: 30 dB.

The signal source oscillator with CSP type is intensity modulated at 0.68 modulation depth. Oscillation frequency is simultaneously modulated with a less than 3 GHz frequency shift [14]. Average signal gain for this frequency-modulated signal is shown in Fig. 4 by filled marks. Signal gain degradation due to undesired frequency modulation is 0.2, 0.6, and 1.7 dB at 20, 25, and 30 dB static signal gains, respectively.

Baseband S/N versus preamplifier input average power P_{in} is shown in Fig. 8. Experimental results in Fig. 7 are replotted using gain saturation characteristics in Fig. 4, taking into account signal gain degradation due to frequency modulation. Solid lines are theoretical values obtained by (11) using −4 dB coupling efficiency η_c in this experiment. Gain saturation characteristics are not included in this calculation. Experimental results are in good agreement with theoretical values in the linear gain region. The dotted-dashed line shows the 21.6 dB baseband S/N which corresponds to a 10^{-9} bit error rate for the optical signal pulse with $\frac{1}{2}$ duty factor and $\frac{1}{2}$ mark density [15]. Minimum detectable average power is experimentally obtained at −43.6, −45.4, and −46.8 dBm at 20, 25, and 30 dB static signal gain, respectively.

Error rate performance for the above preamplifier system was measured in the same experimental setup shown in Fig. 10 in [6]. The signal source oscillator is directly modulated by an alternately mark and space NRZ signal current at 100 Mbits/s to evaluate the S/N performance without pattern effects in the modulation characteristics. Modulation depth was 0.625. Error rate measurement was carried out using the same baseband amplifier as in the S/N measurement and a low-pass filter with 75 MHz cutoff frequency.

Error rate P_e versus preamplifier input average power P_{in} is

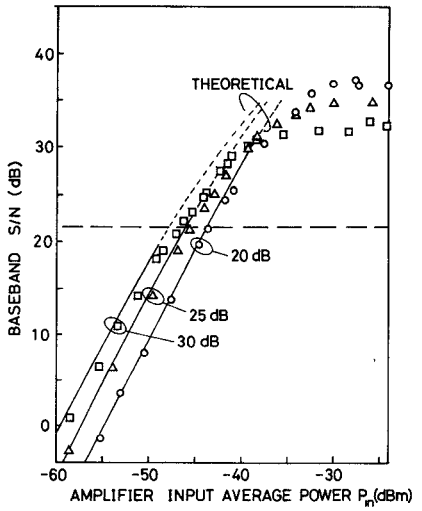

Fig. 8. Baseband *S/N* versus preamplifier input signal average power P_{in}. Dotted-dashed line shows the *S/N* = 21.6 dB.

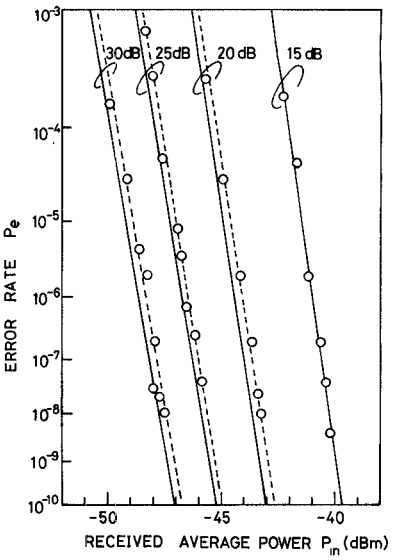

Fig. 9. Error rate P_e in the AlGaAs preamplifier scheme versus preamplifier input average power P_{in} with various signal gain *G* values.

shown in Fig. 9. Preamplifier input power is calculated from the received optical power, taking into account signal gain degradation due to unintended frequency modulation and coupling efficiency η_c, ranging from −4 to −5 dB. Solid lines are theoretical values obtained from the calculated *S/N* using Personick's P_e-*S/N* relation [15]. Minimum detectable powers at 15, 20, 25, and 30 dB static signal gain were measured at −40, −43, −45.3, and −47 dBm, respectively.

Minimum detectable average power to give a 10^{-9} error rate versus preamplifier signal gain is shown in Fig. 10. The solid line represents the theoretical values calculated by (11) with $m = 0.68$ and $\eta_c = -4$ dB. Experimental results, both obtained by *S/N* measurement (shown by open circles) and by error rate measurement (shown by filled circles), are in good agreement with theoretical predictions, within 1 dB error.

The minimum detectable power for the Si-APD direct detection scheme was also measured with $m = 0.625$ to be −39.6 dBm by the error rate evaluation (shown in Fig. 15 as the line *A*). The preamplifier detection scheme with more than 15 dB signal gain improves the minimum detectable power by up to 7.4 dB over the Si-APD direct detection level. −47 dBm minimum detectable power, obtained with 30 dB preamplifier signal gain, corresponds to the direct detection level achieved by the APD with $x = 0.24$.

The spontaneous-spontaneous beat noise reduction is important in the optimized preamplifier performance. The preamplifier is free from gain saturation and signal-spontaneous beat noise, since it is used to amplify a very weak signal.

Noise parameters $n_{sp}^2 \Delta f_2$ and $n_{sp}\chi$ versus input mirror reflectivity R_1 are shown in Fig. 11 for various output mirror reflectivity R_2 values. $n_{sp}^2 \Delta f_2$ and $n_{sp}\chi$ represent the spontaneous-spontaneous beat noise and the signal-spontaneous beat noise, respectively, in the preamplifier at fixed *G* and m_t values. They are calculated by using (5), (6), and (10) at *G* = 20 dB. Solid lines show the noise parameters in the symmetrical cavity structure with $R_1 = R_2$. Dotted, dotted-dashed, and broken lines show noise parameters in the asymmetrical cavity structures whose R_2 is fixed at 0.06, 0.32, and

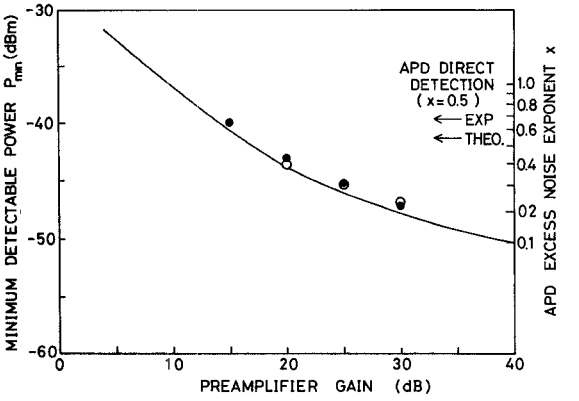

Fig. 10. Minimum detectable average power P_{min} versus preamplifier signal gain *G*. APD direct detection level with excess noise exponent *x* is indicated on the right ordinate by *x* for 0.68 experimental modulation depth in the *S/N* measurement. Experimental and theoretical APD direct detection levels with $m = 0.625$ are indicated by arrows. ○: *S/N* measurement, ●: Error rate measurement.

0.9, respectively. $n_{sp}^2 \Delta f_2$ can be reduced by about 10-20 dB using the narrow-band optical filter to select the gain central longitudinal mode. Baseband *S/N* in the preamplifier system is mainly determined by the spontaneous-spontaneous beat noise represented by $n_{sp}^2 \Delta f_2$. $n_{sp}^2 \Delta f_2$ in the symmetrical cavity structure increases monotonically with reducing the facet reflectivities due to the degradation in the FP filter effect and the gain bandwidth broadening. In the asymmetrical cavity structure, however, $n_{sp}^2 \Delta f_2$ decreases with reducing R_1 and has a minimum value in the $R_1 < R_2$ region due to the above-mentioned two reasons. As R_2 approaches 1, a smaller attainable minimum value for $n_{sp}^2 \Delta f_2$ is obtained at higher R_1. $R_1 = 0.06$ is the optimum reflectivity for the experimented amplifier with $R_2 = 0.32$. Provided that R_2 is set to be 0.9, the minimum value for $n_{sp}^2 \Delta f_2$ is decreased by 9 dB. An extremely asymmetrical cavity structure with low-input and high-output reflectivities is preferable for the preamplifier.

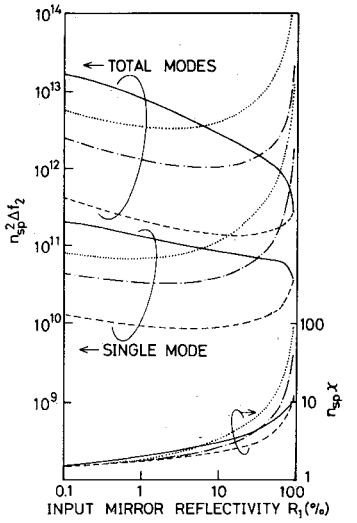

Fig. 11. $n_{sp}^2\Delta f_2$ and $n_{sp}\chi$ versus input mirror reflectivity R_1.
———: $R_2 = R_1$, ·····: $R_2 = 0.06$,
——·——: $R_2 = 0.32$, – – – – –: $R_2 = 0.9$.

$n_{sp}\chi$ decreases by reducing R_1. $n_{sp}\chi$ in the low R_1 region approaches a constant value, independent from R_2.

Minimum detectable average power P_{min} to give a 10^{-9} error rate at the 100 Mbit/s data rate is shown in Fig. 12 as a function of the preamplifier gain. Theoretical values are calculated by (11) with $m = 1$ and $\eta_c = 1$. Solid lines A and broken lines B are P_{min} values for the asymmetrical cavity structure with $(R_1, R_2) = (0.06, 0.32)$ and $(0.01, 0.9)$, respectively. The latter improves P_{min} by 3 dB more than that of the former in the total mode operation. Improvement by 1-7 dB can be expected from the single mode operation. The ideal TW amplifier with $\Delta f_2 = 200$ MHz (shown by C) can improve the minimum detectable power by 14 dB over the APD direct detection level with $x = 0.5$.

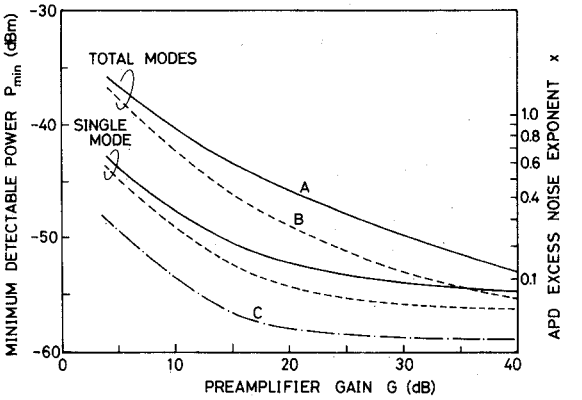

Fig. 12. Minimum detectable average power P_{min} at the 100 Mbit/s data rate versus preamplifier gain G. APD direct detection level with excess noise exponent x is indicated on the right ordinate by x. A: $(R_1, R_2) = (0.06, 0.32)$, B: $(R_1, R_2) = (0.01, 0.9)$, C: ideal TW amplifier with $\Delta f_2 = 200$ MHz.

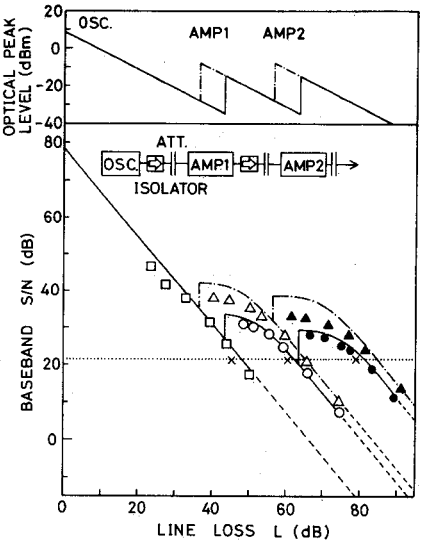

Fig. 13. Peak optical signal level P_{out}^p and baseband S/N versus line loss L. $S/N = 21.6$ dB is indicated by dotted line. S/N measurement – – – □: without repeater ($m = 0.75$), $P_{out}^p = -15.1$ dBm ($m = 0.75$); ○: first repeater output, ●: second repeater output; $P_{out}^p = -8.3$ dBm ($m = 0.68$); △: first repeater output, ▲: second repeater output. Error rate measurement ($m = 0.625$): X.

V. Linear Repeater System Performance

Two repeater amplifiers are used in tandem with an optical attenuator and an isolator in between, as shown by the inset in Fig. 13. Frequency matching between oscillator and two repeaters is carefully carried out concentrating on the temperature control. Experimental conditions are the same as in the preamplifier experiment.

Baseband S/N was measured at various optical signal levels both in front of and behind the optical repeaters. The peak optical signal level and the baseband S/N at the 100 Mbit/s data rate in the system with two repeaters are shown in Fig. 13 as a function of line loss L that can be equalized by the repeater. The repeater amplifiers are biased at $J/J_{th} = 0.94$ where the signal gain is measured at 20 dB and the 3 dB half bandwidth is 4.3 GHz. Unintended frequency modulation is less than 3 GHz [14], which is well within the amplifier bandwidth. S/N performance was experimented with in two systems in which the amplified peak signal level for each repeater is different. The lower amplified peak signal level is -15.1 dBm with 0.75 modulation depth, which is well below the -4.4 dBm saturation output level. The higher amplified peak signal level is -8.3 dBm with 0.68 modulation depth where the signal gain is compressed by 1 dB due to gain saturation. Solid lines and dotted-dashed lines are theoretical values calculated by (17) for each amplified peak signal level and modulation depth. Experimental results are in good agreement with theoretical predictions. In the higher signal level system, measured S/N degradation by 3-6 dB stems from both signal degradation due to gain saturation and noise enhancement due to the shortage of the optical isolation. Baseband S/N behavior behind the amplifier repeater can be explained by the loss dependence of both the beat noise and the shot noise. The S/N value just after the repeater output is determined by the beat noise decreasing with L^{-2}, the same as the baseband signal power. Since shot noise decreases with L^{-1}, the S/N value after the large attenuation is dominated by shot noise and thermal noise. The flat S/N region becomes wider by increasing the number of repeaters k.

Compared to the direct detection system, the optically

repeater system has improved the baseband *S/N* by 6 and 26 dB just after the first and the second repeater outputs, respectively. The regenerative repeater gain, which is defined as the region above $S/N = 21.6$ dB (shown by the dotted line), is increased by 14 and 19 dB using the first and second repeaters, respectively, in the low signal level system. In the high signal level system, 37 dB regenerative repeater gain is obtained.

Fig. 14 shows the NRZ pulse pattern optical signal at 100 Mbits/s. Input signal (a) is linearly amplified by the first (b) and the second (c) repeaters.

Error rate characteristics were also measured at various signal levels in front of and behind the optical repeaters whose amplified peak signal level is −15.1 dBm. The signal source oscillator is directly modulated by an alternately mark and space NRZ pulse current with 0.625 modulation depth at the 100 Mbit/s data rate. Error rate P_e versus received average power P_{in} is shown in Fig. 15. Here, received power P_{in} behind the first and the second repeaters is expressed by the average power corresponding to that in the direct detection scheme by subtracting 20 and 40 dB, respectively, from the measured power. Solid lines show the theoretical values calculated by (17) with $m = 0.625$. Error rate characteristics indicated by *A*, *B*, and *C* are measured in the direct detection scheme and in the optically repeatered system with one and two repeaters, respectively. Experimental results are in reasonable agreement with theoretical predictions. The floor appears in the $P_e - P_{in}$ characteristics of the second repeater output. The theoretical floor is influenced by the flat *S/N* behavior. The experimental floor seems to stem from the matching frequency fluctuation between oscillator and repeaters.

Regenerative repeater gain, increased by the first and the second repeaters, is measured at 15 and 18.3 dB, respectively. Error rate measurement results are also indicated in Fig. 13 by marks with a cross.

The baseband *S/N*, just after the repeater output for the perfect on-off modulation signal at 100 Mbits/s, is shown in Fig. 16 as a function of the number of repeaters *k*. At the amplified peak optical level of −14.5 dBm, seven repeaters with $(R_1, R_2) = (0.06, 0.32)$ can theoretically be inserted between regenerative terminal repeaters with maintaining $S/N \geqq 21.6$ dB (shown by the dotted line). The number of repeaters can be increased to 36 and 130 by using the FP repeaters with a narrow-band optical filter and the ideal TW repeaters with $\Delta f_1 = \Delta f_2 = 200$ MHz, respectively. FP repeaters, operating in total modes at $P^p_{out} = -14.5$ dBm, have spontaneous-spontaneous beat noise comparable to the signal-spontaneous beat noise at $k = 1$. *S/N* in the above repeater system decreases with k^{-2} due to the accumulation of the spontaneous-spontaneous beat noise. Ideal TW repeaters are operating in the signal-spontaneous beat noise limit. Their *S/N* is inversely proportional to *k*. The number of repeaters with maintaining $S/N \geqq 21.6$ dB can be increased to 63 at the −5 dBm amplified peak optical level, which is just below the saturation output power for the FP repeater.

In the linear repeater system with low signal operation, the spontaneous-spontaneous beat noise represented by $n_{sp}^2 \Delta f_1 \chi$ is important because it increases with $k(k-1)$. The $n_{sp}^2 \Delta f_1 \chi$ behavior for various (R_1, R_2) configurations is the same as that

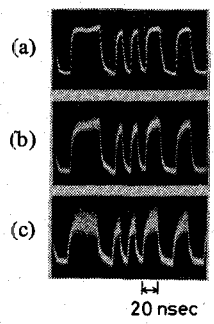

Fig. 14. NRZ pulse pattern optical signal at 100 Mbits/s. (a) Input signal. (b) Amplified signal at the first repeater output. (c) Amplified signal at the second repeater output.

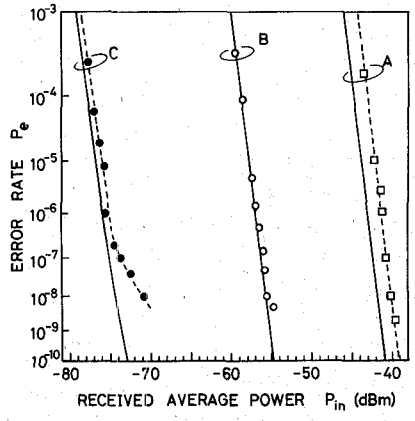

Fig. 15. Error rate P_e in the two linear repeater system versus received averaged power P_{in}. P_{in} is expressed as the average power corresponding to that in the direct detection scheme. Modulation depth is 0.625. *A*: Without repeater (APD direct detection scheme). *B*: First repeater output. *C*: Second repeater output.

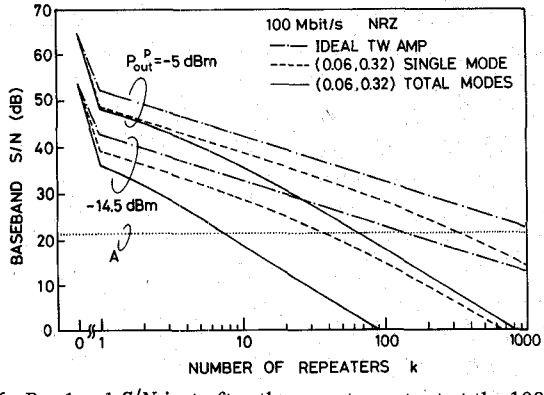

Fig. 16. Baseband *S/N* just after the repeater output at the 100 Mbit/s data rate as a function of the number of repeaters *k*. $S/N = 21.6$ dB is indicated by dotted line *A*.

for $n_{sp}^2 \Delta f_2$, shown in Fig. 11, except that $n_{sp}^2 \Delta f_1 \chi$ has a 6 dB larger value than $n_{sp}^2 \Delta f_2$. *S/N* degradation *D*, due to the spontaneous-spontaneous beat noise, can be reduced by increasing the amplified signal level, which is limited by saturation output power $P_{3\,dB}$. Baseband *S/N* is proportional to the amplified signal level in the signal-spontaneous beat noise limit where *D* is determined by $n_{sp}\chi$. $P_{3\,dB}$ and $n_{sp}\chi$ are the most important parameters for the repeater amplifier. $n_{sp}\chi$ decreases with reducing input mirror reflectivity R_1, as shown in Fig. 11. High-output mirror reflectivity, which was prefer-

able for the preamplifier, is inadequate from the high $P_{3\ dB}$ viewpoint. Optimum cavity configuration for the repeater amplifier is presumably the symmetrical low-Q cavity structure or the asymmetrical configuration with low-input and adequately high-output mirror reflectivities. In the latter configuration, R_2 is determined by the tradeoff relation between the high saturation output power and the low spontaneous-spontaneous beat noise. In both configurations, the use of a narrow-band optical filter is indispensable for reducing the spontaneous-spontaneous beat noise and avoiding the gain saturation due to the accumulated spontaneous emission.

VI. Conclusion

Baseband S/N and error rate characteristics in AlGaAs laser preamplifier and linear repeater systems were studied theoretically and experimentally.

The optical preamplifier has improved the minimum detectable power by 7.4 dB over the Si-APD direct detection level. Further improvement by 6-9 dB can be expected from the FP amplifier with a narrow-band optical filter or the ideal TW amplifier. Integration of an optical preamplifier with a p-i-n photodiode (PD) or APD for reducing the coupling loss may be a promising candidate for improved receiver sensitivity design.

The semiconductor laser linear repeater system can increase the regenerative repeater gain by 120 dB using seven repeaters at the -14.5 dBm amplified peak signal level. Higher signal level operation without gain saturation would expand the regenerative repeater spacing up to 4000 and 66 000 km for the FP cavity repeaters and the ideal TW repeaters, respectively. The semiconductor laser linear repeater system offers a possibility for use in transoceanic fiber cable systems, wherein all the undersea repeaters can be constructed using only the optical linear amplifier. It also may be used in terrestrial long distance systems.

Optimum design for the optical amplifier differs in actual usage. The preamplifier is desired to have an extremely asymmetrical cavity configuration with low-input and high-output mirror reflectivities. Repeater amplifiers are desired to have a low-Q cavity with low input mirror reflectivity and a higher saturation output power level.

Frequency matching between the input signal and the amplifier FP mode is serious in the linear repeater system. Feedback control loops, such as AFC and AGC, are indispensable to the FP repeaters. Traveling-wave amplifiers settle the frequency-matching problem and offer a possibility of common amplification for a wavelength-multiplexed signal within a wide gain spectrum. An optical isolator and a narrow-band optical filter compatible with a single mode fiber and low insertion loss are indispensable for the high-performance optical direct amplification systems. It is also desired to realize the amplifier without signal gain dependence on input signal polarization.

Acknowledgment

The authors wish to thank A. Kawana for useful suggestions and discussions.

References

[1] Y. Yamamoto, "Noise and error rate performance of semiconductor laser amplifiers in PCM-IM optical transmission systems," *IEEE J. Quantum Electron.*, vol. QE-16, pp. 1073-1081, Oct. 1980.

[2] G. Zeidler and D. Schicketanz, "Use of laser amplifier in a glass-fiber-communication systems," *Siemens Forsh. Entwickl.-Ber.*, vol. 2, no. 4, pp. 227-234, 1973.

[3] Y. Yamamoto and T. Kimura, "Coherent optical fiber transmission systems," *IEEE J. Quantum Electron.*, vol. QE-17, pp. 919-935, June 1981.

[4] F. Favre, L. Jeunhomme, I. Joindot, M. Monerie, and J. C. Simon, "Progress toward heterodyne-type single-mode fiber communication systems," *IEEE J. Quantum Electron.*, vol. QE-17, pp. 897-906, June 1981.

[5] Y. Yamamoto and H. Tsuchiya, "Optical receiver sensitivity improvement by a semiconductor laser preamplifier," *Electron. Lett.*, vol. 16, pp. 233-235, 1980.

[6] Y. Yamamoto, "Characteristics of AlGaAs Fabry-Perot cavity type laser amplifiers," *IEEE J. Quantum Electron.*, vol. QE-16, pp. 1047-1052, Oct. 1980.

[7] T. Mukai and Y. Yamamoto, "Noise characteristics of semiconductor laser amplifiers," *Electron. Lett.*, vol. 17, pp. 31-33, Jan. 1981.

[8] T. Mukai and Y. Yamamoto, "Noise in an AlGaAs semiconductor laser amplifiers," *IEEE J. Quantum Electron.*, vol. QE-18, pp. 564-575, Apr. 1982.

[9] S. Kobayashi and T. Kimura, "Gain and saturation power of resonant AlGaAs laser amplifier," *Electron. Lett.*, vol. 16, pp. 230-232, 1980.

[10] T. Mukai and Y. Yamamoto, "Gain, frequency bandwidth, and saturation output power of AlGaAs laser amplifiers," *IEEE J. Quantum Electron.*, vol. QE-17, pp. 1028-1034, June 1981.

[11] H. C. Casey and M. B. Panish, *Heterostructure Lasers.* New York: Academic, 1978.

[12] Y. Yamamoto, S. Saito, and T. Mukai, "AM and FM quantum noise in semiconductor lasers II: Comparison of theoretical and experimental results for AlGaAs lasers," *IEEE J. Quantum Electron.*, to be submitted.

[13] K. Aiki, M. Nakamura, T. Kuroda, J. Umeda, R. Ito, N. Chinone, and M. Maeda, "Transverse mode stabilized AlGaAs injection laser with channeled-substrate-planar structure," *IEEE J. Quantum Electron.*, vol. QE-14, pp. 89-94, Feb. 1978.

[14] S. Kobayashi, Y. Yamamoto, M. Ito, and T. Kimura, "Direct frequency modulation in AlGaAs semiconductor lasers," *IEEE J. Quantum Electron.*, vol. QE-18, pp. 582-595, Apr. 1982.

[15] S. D. Personick, "Receiver design for digital fiber optic communication systems, I," *Bell Syst. Tech. J.*, vol. 52, pp. 843-874, 1973.

Takaaki Mukai, for a photograph and biography, see p. 421 of the April 1982 issue of this Transactions.

Yoshihisa Yamamoto (S'75-M'80), for a photograph and biography, see p. 421 of the April 1982 issue of this Transactions.

Tatsuya Kimura (S'63-M'68-SM'78), for a photograph and biography, see p. 65 of the January 1982 issue of the Journal of Quantum Electronics.